ORIGINAL ARTICLE

Chemical composition of biotite from the Lar Cu-Mo prospect igneous rocks, Southeastern part of Iran

Rahele Moradi[1], M. Boomeri[1], K. Nakashima[2]

[1]Department of Geology, Faculty of Sciences, University of Sistan and Baluchestan, Zahedan, Iran,
[2]Department of Earth and Environmental Sciences, Faculty of Science, Yamagata University, Yamagata, Japan

Abstract

Background and Objective: The Lar Cu-Mo prospect is located in Sistan suture zone, southeast of Iran. In this study, the chemical composition of biotite is determined using electron probe micro-analyzer in shoshonitic igneous rocks. Shoshonitic rocks are syenitic to monzonitic in composition that can be divided into the granular and porphyroid groups. **Methods:** Studying biotites generally occurs as primary and secondary types. The primary biotites are large poikilitic phenocrysts associated with Fe-Ti oxides, giving the rocks a spotted texture. In addition, secondary biotites show varying size, color, and shape. All of the Lar analyzed biotites are Mg-and Ti-rich and F- and Cl-poor. Analyses of the Lar biotites suggested that crystallization took place at an average temperature of 731°C and 640°C for primary and secondary samples, respectively. **Results:** Estimation of the oxygen fugacity, based on chemical composition and Fe^{3+} content of biotite, shows that the oxygen fugacity was limited in fayalite-magnetite quartz to middle of HM buffers in quality and was about 10^{-12} to 10^{-14} bar in quantity for primary and secondary type, respectively. Halogen fugacity ratios in biotite show that the Lar porphyroid rocks (ore-bearing) are affected mainly by meteoric water than granular type (barren). Calculated halogen fugacity values for biotite in the Lar Cu-Mo prospect are consistent with many other porphyry copper-forming systems. **Conclusion:** The Lar Cu-Mo prospect was formed by the hydrothermal activity related to the syenitic to monzonitic porphyroid igneous rocks with shoshonitic nature which introduces the Lar igneous complex volcanic sequence. The hydrothermal alterations are limited and occurred as silicic, potassic, phyllic, propylitic, and argillic. Hypogene sulfide minerals mainly occur as disseminated and sulfidic and silicic veins and veinlets consisting of chalcopyrite, bornite, molybdenite, and minor pyrite. Biotite as main ferromagnesian mineral of host rocks occurs as primary in less altered rocks and secondary in the alteration areas.

Key words: Biotite chemistry, Lar Cu-Mo prospect, shoshonitic igneous rocks, Sistan suture zone, Southeast of Iran

INTRODUCTION

The Lar Cu-Mo prospect is located at 20 km North of Zahedan, Southeastern part of Iran [Figure 1a]. The prospect is mainly a part of the Lar igneous complex (LIC). Although the LIC has been subject of several petrological and geochemical MSc thesis and projects,[1-5] we have few published information about the Lar Cu-Mo prospect[6-8] that is the most complete study about mineralization in the Lar Cu-Mo prospect. Based on Moradi (2016), the Lar Cu-Mo prospect is a porphyry type deposit regarding to size, grade, and the host rock and different regarding to alteration types, mineralization style, and fluid characteristics. The mineralization covers an area of 0.75 km^2 and contains several million tonnes of mineralized rocks averaging 0.16% Cu and 0.01% Mo.[9]

In this study, in addition to describing geological and mineralogical features of the Lar Cu-Mo prospect, we present new biotite electron probe micro-analyzer data due to the composition of biotite reflects the chemical characteristics of the rocks, associated hydrothermal fluids, and the physicochemical conditions of their formation.[10-13] With data obtained, the chemical composition of biotite and its halogen chemistry, temperature, and oxygen fugacity values were

Address for correspondence:
Rahele Moradi, Department of Geology, Faculty of Sciences, University of Sistan and Baluchestan, Zahedan, Iran. Phone: +91-9151400276.
E-mail: rmoradi@pgs.usb.ac.ir

Received: 12-07-2017
Revised: 28-08-2017
Accepted: 08-09-2017

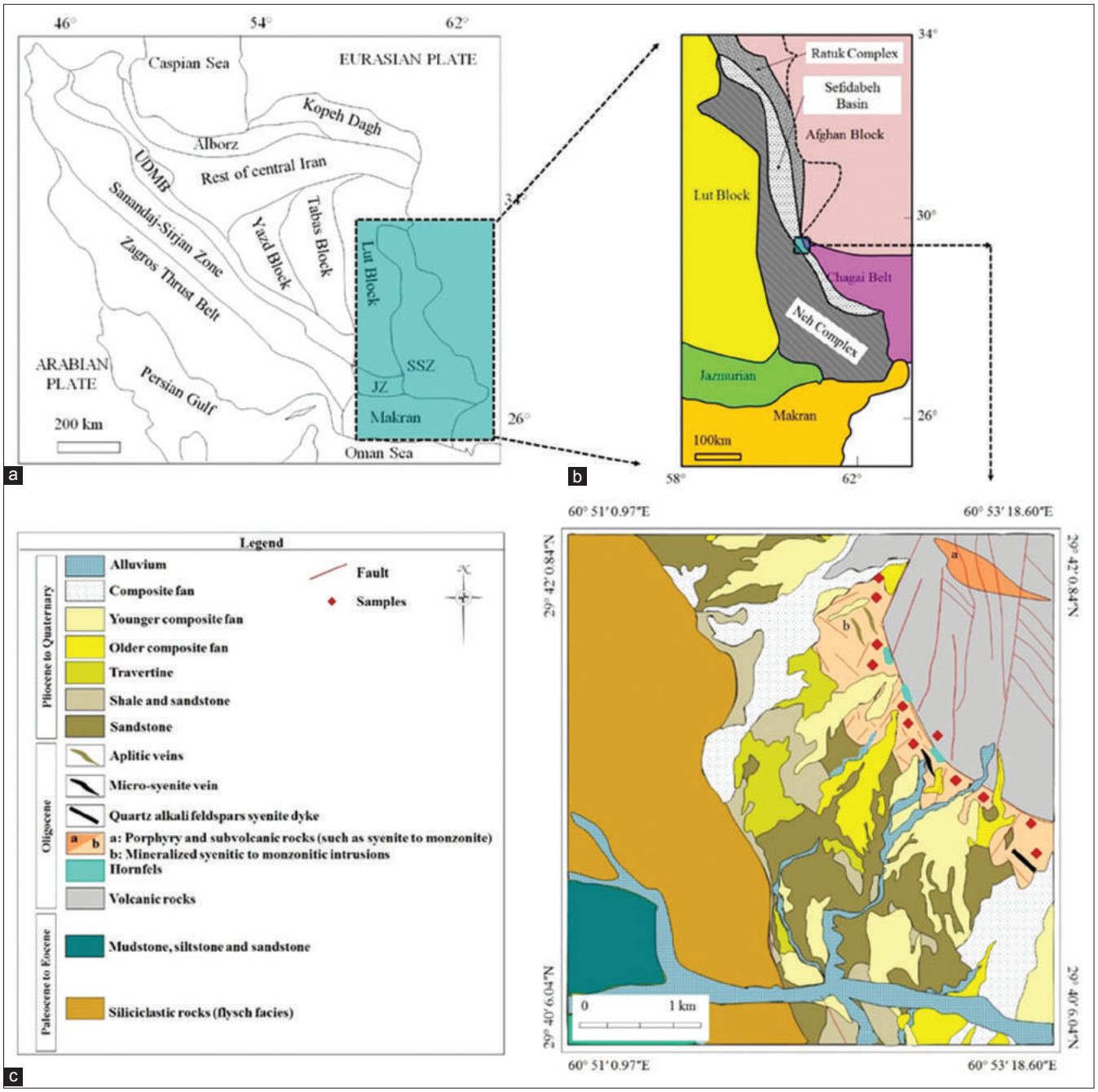

Figure 1: (a) Geological maps of a main tectonostratigraphic units of Iran and location of the Sistan suture zone (SSZ),[14] (b) geological subdivisions of the SSZ consist of Neh-Ratuk accretionary prism and Sefidabeh forearc basin between blocks of Lut and Afghan[15] and location of the Lar Cu-Mo prospect, (c) the Lar Cu-Mo prospect[16]

calculated in the shoshonitic igneous rocks and alteration zones. All these helped constrain the physicochemical conditions of the Lar Cu-Mo prospect.

MATERIALS AND METHODS

One hundred samples were collected from the surface and drill holes. Standard thin-polished sections were made out of the samples. The samples were examined by polarized microscope for petrographic descriptions at the University of Sistan and Baluchestan, Zahedan, Iran. Ten and five thin-polished sections were selected from less-altered igneous rocks (syenitic to monzonitic igneous rocks with granular and porphyritic textures, andesite, and tuff) and alteration areas (potassic, propylitic, and argillic), respectively, for electron microprobe analysis to determine the biotite composition.

In general, there are two types of biotites in the Lar Cu-Mo prospect, namely, primary and secondary biotites. They were then analyzed by the automated JEOL JXA-8600 superprobe of Yamagata University with accelerating voltage of 15 kV,

a beam current of 20 nA, a beam diameter of about 5 μm, detection limits of 0.05 wt. %, and maximum 40 s counting interval. The diameter of the focused electron beam is about 5 μm. Data were processed by an online computer using the oxide ZAF in the XM-86 PAC program of JEOL. Calibration standards for the mentioned minerals were apatite, wollastonite, albite, adularia, synthetic SiO_2, TiO_2, Al_2O_3, Fe_2O_3, MnO, MgO, CaF_2, and NaCl. In each sample, several grains and points of biotite were analyzed according to textural relations, and an average of the analytical results was taken to represent the typical composition of the biotite in each sample. The chemical composition and formula calculation of biotite based on 22 atoms of oxygen are listed in Table 1.

The Lar Cu-Mo prospect is geologically located in the Sistan suture zone (SSZ) [Figures 1a and b]. The SSZ is known as remnants of an oceanic basin that extends as an N–S trending belt over more than 700 kilometers along the border area among Iran, Afghanistan, and Pakistan. Based on Camp and Griffis (1982)[7] the SSZ is characterized by the following features: (A) Ophiolites, (B) Flysch-type rocks, and (C) non-ophiolitic igneous rocks that are different in age, composition, and genesis and can be divided according to their age and nature as follows:

1. Eocene calc-alkaline rocks of the accretionary prism that are known as indicators of subduction of the Lut block beneath the Afghan block.[17]
2. Early Oligocene Zahedan calc-alkaline I-, rare S, and

Table 1: Representative average chemical composition (wt. %) and structural formula of biotite in the Lar prospect

Alterations	**Rocks**								
	Syenite	**Syenite**	**Quartz syenite**	**Monzonite**	**Andesite**	**Tuff**	**Potassic**	**Propylitic**	**Argillic**
Texture	Porphyry	Granular	Porphyry	Porphyry	Porphyry	Porphyry	Porphyry	Porphyry	Porphyry
Number of samples	2	3	1	2	1	1	3	1	1
Number of points	6	9	8	9	9	7	71	21	15
	Av.	Av.	Av.	Av.	Av.	Av.	Av.	Av.	Av.
SiO_2	38.35	38.98	38.10	39.14	38.21	38.95	37.33	36.77	36.87
TiO_2	3.55	3.59	3.68	3.44	3.33	3.23	2.13	1.73	2.12
Al_2O_3	15.16	14.65	15.15	14.66	15.00	15.39	14.50	14.46	14.40
FeO	16.41	16.03	16.87	16.18	17.27	16.05	15.84	16.67	15.78
MnO	0.20	0.26	0.25	0.28	0.24	0.24	0.19	0.28	0.25
MgO	15.10	15.20	14.80	15.01	14.65	15.58	14.15	13.78	14.55
CaO	0.03	0.04	0.04	0.09	0.03	0.04	0.12	0.17	0.32
Na_2O	0.12	0.13	0.17	0.12	0.14	0.23	0.26	0.26	0.27
K_2O	9.14	9.02	9.03	8.83	8.58	8.55	8.96	8.85	8.15
BaO	0.08	0.11	0.14	0.14	0.23	0.22	0.11	0.14	0.12
Cl	0.09	0.11	0.07	0.09	0.04	0.03	0.06	0.03	0.15
F	0.31	0.24	0.22	0.40	0.23	0.23	0.30	0.16	0.31
O=–Cl	0.02	0.02	0.02	0.02	0.01	0.01	0.01	0.01	0.03
O=–F	0.13	0.10	0.09	0.17	0.10	0.10	0.13	0.07	0.13
H_2O	4.05	4.07	4.06	4.04	4.04	4.11	3.86	3.85	3.83
Total	102.44	102.31	102.48	102.23	101.89	102.75	97.67	97.08	96.96
Numbers of cations on the basis of 22 O									
Si	5.56	5.64	5.54	5.66	5.58	5.60	5.68	5.66	5.63
^{IV}Al	2.44	2.36	2.46	2.34	2.42	2.40	2.32	2.34	2.37
T site	8.00	8.00	8.00	8.00	8.00	8.00	8.00	8.00	8.00
^{VI}Al	0.15	0.14	0.14	0.16	0.17	0.21	0.28	0.29	0.23
Ti	0.39	0.39	0.40	0.37	0.37	0.35	0.24	0.20	0.24
Fe	1.99	1.94	2.05	1.96	2.11	1.93	2.01	2.15	2.02

(*Contd...*)

Table 1: (*Continued*)

Alterations	Rocks								
	Syenite	Syenite	Quartz syenite	Monzonite	Andesite	Tuff	Potassic	Propylitic	Argillic
Mn	0.02	0.03	0.03	0.03	0.03	0.03	0.02	0.04	0.03
Mg	3.26	3.28	3.21	3.24	3.19	3.34	3.21	3.16	3.31
O site	5.81	5.78	5.83	5.76	5.86	5.86	5.77	5.84	5.84
Ca	0.00	0.01	0.01	0.01	0.00	0.01	0.02	0.03	0.05
Na	0.03	0.04	0.05	0.03	0.04	0.06	0.08	0.08	0.08
K	1.69	1.67	1.67	1.63	1.60	1.57	1.74	1.74	1.59
Ba	0.00	0.01	0.01	0.01	0.01	0.01	0.01	0.01	0.01
A site	1.73	1.71	1.73	1.68	1.64	1.64	1.83	1.84	1.72
Cl	0.01	0.01	0.01	0.01	0.00	0.00	0.01	0.00	0.02
F	0.07	0.05	0.05	0.09	0.05	0.05	0.07	0.04	0.07
OH	3.92	3.93	3.94	3.90	3.94	3.94	3.92	3.96	3.91
X_{Mg}	0.62	0.63	0.61	0.62	0.60	0.63	0.61	0.60	0.62
X_{phl}	0.57	0.57	0.56	0.57	0.55	0.59	0.59	0.56	0.63
X_{sid}	0.21	0.18	0.22	0.18	0.22	0.20	0.19	0.22	0.18
X_{an}	0.22	0.25	0.22	0.25	0.23	0.21	0.22	0.23	0.19
Biotite halogen composition									
log X_F/X_{OH}	−1.75	−1.90	−1.90	−1.64	−1.90	−1.90	−1.75	−2.00	−1.75
log X_{Cl}/X_{OH}	−2.59	−2.59	−2.60	−2.59	-	-	−2.59	-	−2.29
log X_F/X_{Cl}	0.85	0.70	0.70	0.95	-	-	0.85	-	0.54
log $(f_{H2O})/(f_{HF})$	5.18	5.30	5.31	5.09	5.37	5.40	5.47	5.77	5.52
log $(f_{H2O})/(f_{HCl})$	4.74	4.73	4.73	4.75	-	-	4.88	-	4.61
log $(f_{HF})/(f_{HCl})$	−1.07	−1.20	−1.20	−0.97	-	-	−1.29	-	−1.68
IV (F)	2.75	2.90	2.88	2.64	2.87	2.92	2.77	2.98	2.82
IV (Cl)	−3.52	−3.52	−3.49	−3.52	-	-	−3.55	-	−3.94
IV (F/Cl)	6.28	6.42	6.38	6.16	-	-	6.32	-	6.77
T°C	727	733	726	719	703	710	643	618	643

OH is calculated by OH=4−(Cl+F); X_{Mg}=Mg/Sum of octahedral cations; IV: Intercept value. IV (F), IV (Cl), IV (F/Cl), log $(f_{H2O})/(f_{HF})$, log $(f_{H2O})/(f_{HCl})$, and log $(f_{HF})/(f_{HCl})$ were calculated using the equations of Munoz (1984, 1992); X_F, X_{Cl}, X_{OH}, X_{sid}, and X_{an} are the mole fractions of F, Cl, OH, siderophyllite, and annite in biotite, respectively

hybrid-type granitoids related to subduction and collision events in the area.[18-26]

3. Oligocene to middle Miocene alkaline and calc-alkaline igneous rocks from Zahedan to Nehbandan cities.[7]
4. Quaternary volcanic rocks like Mount Taftan related to the Makran active subduction of the Oman oceanic lithosphere under the Makran accretionary prism and the SSZ.[27]

The SSZ was divided into Neh-Ratuk accretionary prism and Sefidabeh forearc basin.[7] The LIC is located in the Sefidabeh forearc basin. It is a late Oligocene elliptical (8 by 5 km in plan view) igneous complex that is hosted by flysch-type rocks.

The Lar Cu-Mo prospect is located in the western and southwestern part of the LIC and consist of flysch-type rocks, igneous rocks, silicic veins, and silicic veinlets [Figure 1c]. Igneous rocks in the mineralized area are two types of extrusive and intrusive rocks that are shoshonitic in nature.[27] The extrusive rocks occur as lava and pyroclastic rocks and lay on the flysch-type rocks. The intrusive rocks occur as stock and dikes. The intrusive stocks are mainly pinkish-to-grayish porphyroid and granular syenite and monzonite. These rocks have been invaded by mineralized and non-mineralized silicic veins and veinlets and a few aplitic and micro-syenitic dikes. There are structurally at least two fault and fracture systems in the mineralized area with NW-SE and NE-SW trends. The NW-SE system is mainly associated with mineralization and has been cut by the younger NE-SW system.

The mineralized area has a different color from surrounded non-mineralized rocks due to hypogene and later supergene alterations [Figure 2a]. The volcanic rocks and hornfels,

especially on the eastern side of the mineralized area, have dark color [Figure 2a]. The supergene mineralization is characterized by the presence of iron hydroxides, Cu-carbonates, and secondary sulfides, such as chalcocite and covellite that partially replaced the hypogene minerals, such as chalcopyrite and bornite, along the fractures. They are often associated with tectonized domains, and they are more intense in the faulted and fractured zones and directions. The hypogene alteration is mainly characterized by quartz formation mainly as silicic vein and veinlets. However, there is no alteration pattern in the Lar mineralized zone like the typical porphyry Cu deposits; there are evidence of potassic, propylitic, and phyllic hypogene alterations. The potassic alteration zone is characterized by the veins containing biotite and K-feldspar associated with bornite, chalcopyrite, and (or) molybdenite. It seems that plagioclase was usually replaced by K-feldspar in the host rocks. Propylitic alteration is more widespread in peripheral parts of the mineralized zone, especially in the hornfels and metavolcanic rocks, where epidote, calcite, chlorite, and minor sericite partially replaced magmatic pyroxene, hornblende, and biotite. Minor actinolite was formed along the cleavage of the primary amphibole in a few samples. Argillic alteration locally occurs in outcrops and shallow depths.

The Cu-Mo mineralization is primarily associated with silicic veins and veinlets that occur in porphyroid syenite and monzonite [Figure 2b and c]. In general, according to the paragenetic sequence, the predominant primary sulfides are pyrite, chalcopyrite, molybdenite, and bornite, followed by magnetite, minor native copper, and enargite. Chalcocite, covellite, malachite, azurite, hematite, and limonite are the secondary minerals developed from the primary ones through weathering. Quartz is the dominant gangue minerals.

As mentioned above, the rock units in the mineralized area are mainly igneous rocks. The syenitic to monzonitic rocks is dominantly medium-to-coarse-grained, porphyroid and occasionally granular and cataclastic in texture. There is extreme variation in the ratio of phenocrysts to groundmass in porphyroid syenite to monzonite as the groundmass ratio is <30%. These rocks consist of K-feldspar, plagioclase, biotite, apatite, titanite, clinopyroxene, amphibole, quartz, epidote, and opaque minerals. In general, biotite in the Lar prospect porphyroid and granular intrusive rocks occurs as phenocrysts, tiny crystals in the groundmass, and inclusions in the other minerals [Figure 3a]. The biotite phenocrysts are mainly brown-to-green in color, varying in texture, shape, and size, and they are partially replaced by chlorite. The biotite

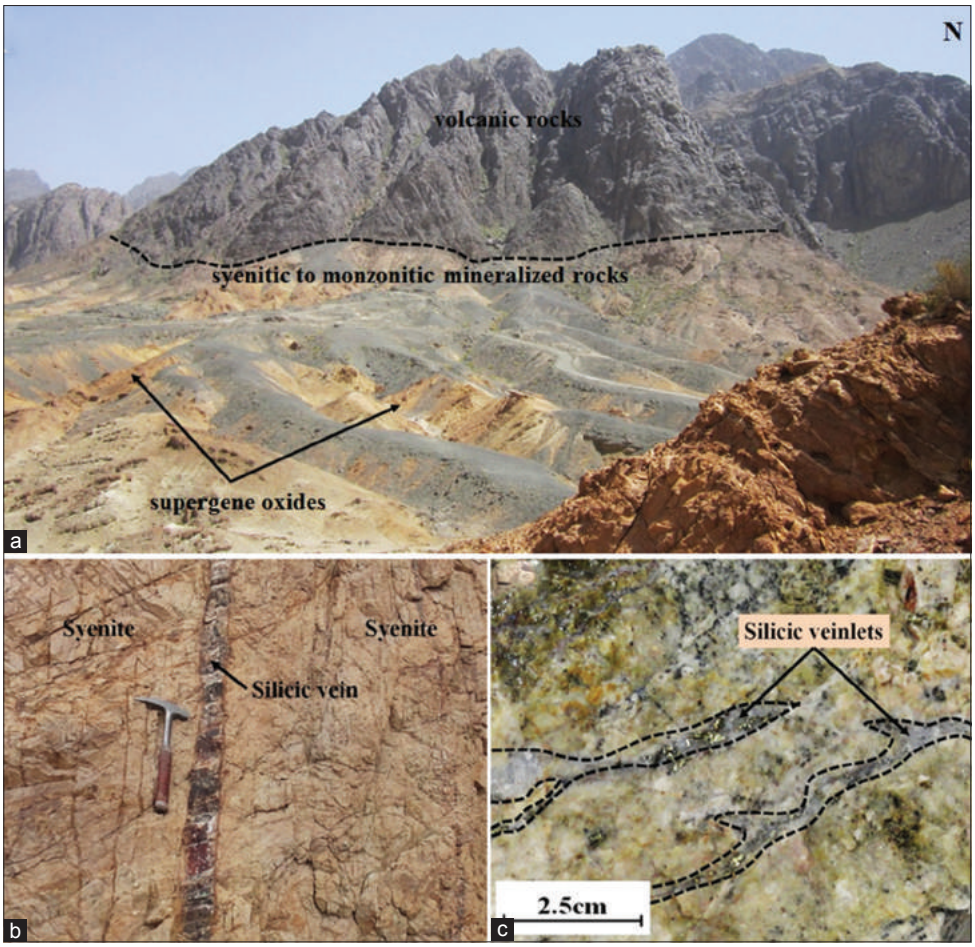

Figure 2: Field photographs of the (a) LIC and Lar Cu-Mo mineralized area, (b) mineralized silicic vein, and (c) mineralized silicic veinlets

crystals are weakly to strongly deformed, bent, and occur usually as isolated bands due to mylonitization [Figure 3b] and have inclusions of plagioclase, biotite, titanite, apatite, pyroxene, and opaque minerals [Figure 3c]. It seems that most of the biotites are secondary biotite as they occur in open spaces and veins. The biotite is sometimes surrounded Fe-Ti oxides [Figure 3d].

The extrusive rocks are mainly trachyte, latite, tuff, and andesite with porphyry texture. The phenocrysts are sanidine, plagioclase, augite, hornblende, biotite, quartz, and opaque minerals that consisting of 50% of the rock volume. The groundmass is composed of fine-grained crystals of feldspar as major mineral and minor ferromagnesian minerals.

RESULTS

A total of 32, 16, and 107 points were analyzed on the biotite phenocrysts of intrusive, extrusive, and altered samples (from potassic, propylitic, and argillic areas), respectively [Table 1].

Biotite compositions, when referred to Al versus Fe/(Fe+Mg) diagram (Rieder *et al*., 1998)[28] [Figure 4a], clearly plot in the biotite field near to the biotite and phlogopite line boundary. The biotites fall in the field of primary and re-equilibrated, respectively [Figure 4b], and have a narrow range in chemical composition of SiO_2, Al_2O_3, TiO_2, and MgO. It seems that the biotites are Mg- and Ti-rich and F- and Cl-poor and fall into the field of calk alkaline orogenic area [Figure 4c and d].

The biotites have fluorine and chlorine contents ranging from 0.22-0.40 and 0.07-0.11, 0.23 and 0.03-0.04, 0.16-0.31 and 0.03-0.15 wt. %, in intrusive, extrusive rocks and samples of alteration areas, respectively.

The concentration of Ti and Ti/Fe^{2+} is very sensitive in biotite to temperature, making it possible to use biotite to obtain reliable temperature estimation in igneous and metamorphic rocks.We used the empirical $Ti\text{-}Fe^{2+}$ geo-thermometer of Luhr *et al.* to calculate the biotite precipitation temperatures [Table 1]. Biotite compositions from the Lar samples show average temperature of 731°C and 640°C in primary and secondary samples, respectively, with the following equation:[29,30]

$$T(^{\circ}K) = \frac{838}{\left(1.0337 - \frac{Ti}{Fe^{2+}}\right)}$$

The biotite compositions can be used to discriminate qualitative evaluation of oxygen fugacity. According to Wones and Eugster (1965) diagram, the comparison of biotite compositions with common oxygen buffers (quartz-fayalite-magnetite [QFM]; nickel-nickel oxide [NNO] and hematite-magnetite [HM]) shows that the Lar biotites are mostly located between QFM to middle of HM buffers [Figure 5a]. The samples plotting between the NNO and HM buffers are related to more magnetite and titanite-bearing rocks in the Lar prospect, indicating fairly oxidizing conditions. Moreover, other samples with more ilmenite and plot in the field of QFM represent a more reducing conditions during crystallization. A qualitative estimation of oxygen fugacity can be obtained using the Fe/(Fe+Mg) value of biotite in $f(O_2)$ - T space for biotite + K-feldspar + magnetite equilibrium (Wones and Eugster, 1965) [Figure 5b]. According to the reasonable average crystallization temperatures of 731°C and 640°C for the Lar biotites, estimated $f(O_2)$ values are about 10^{-12}-10^{-14} bars in primary and secondary biotites, respectively [Figure 5b].[31]

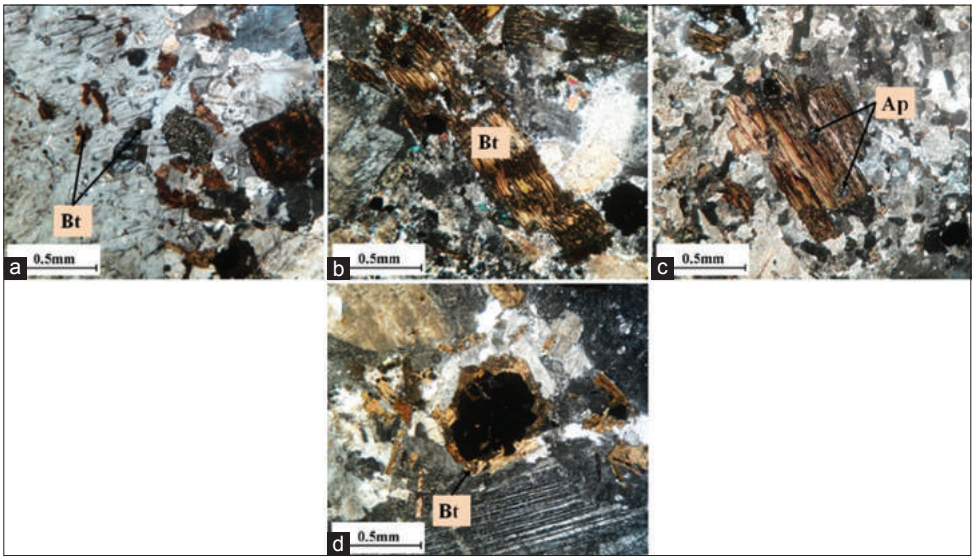

Figure 3: Cross-polarized light photomicrographs of (a) K-feldspar megacryst poikilitically encloses small grains of plagioclase, biotite, titanite, apatite, pyroxene, and opaques, (b) biotite with deformed cleavage, (c) biotite phenocrysts with inclusions of apatite, titanite, and opaque minerals, (d) Fe-Ti oxides surrounded by rime of biotites

Biotite composition is useful in the calculation of the fluorine and chlorine fugacities for responsible hydrothermal fluids of mineralization and hydrothermal alteration processes, represented by log $(f_{HF})/(f_{H2O})$ and log $(f_{HCl})/(f_{H2O})$, respectively.[32,33] Halogen fugacity can be computed using equations of Munoz,which are based on the revised coefficients for the halogen–hydroxyl exchange.[33,34] These equations are as follows:

- log $(f_{H2O})/(f_{HF})^{fluid}$=1000/T $(2.37+1.1\ (X_{Mg})^{biotite})+0.43-$ log $(X_F/X_{OH})^{biotite}$,
- log $(f_{H2O})/(f_{HCl})^{fluid}$=1000/T $(1.15+0.55\ (X_{Mg})^{biotite})+0.68-$ log $(X_{Cl}/X_{OH})^{biotite}$,

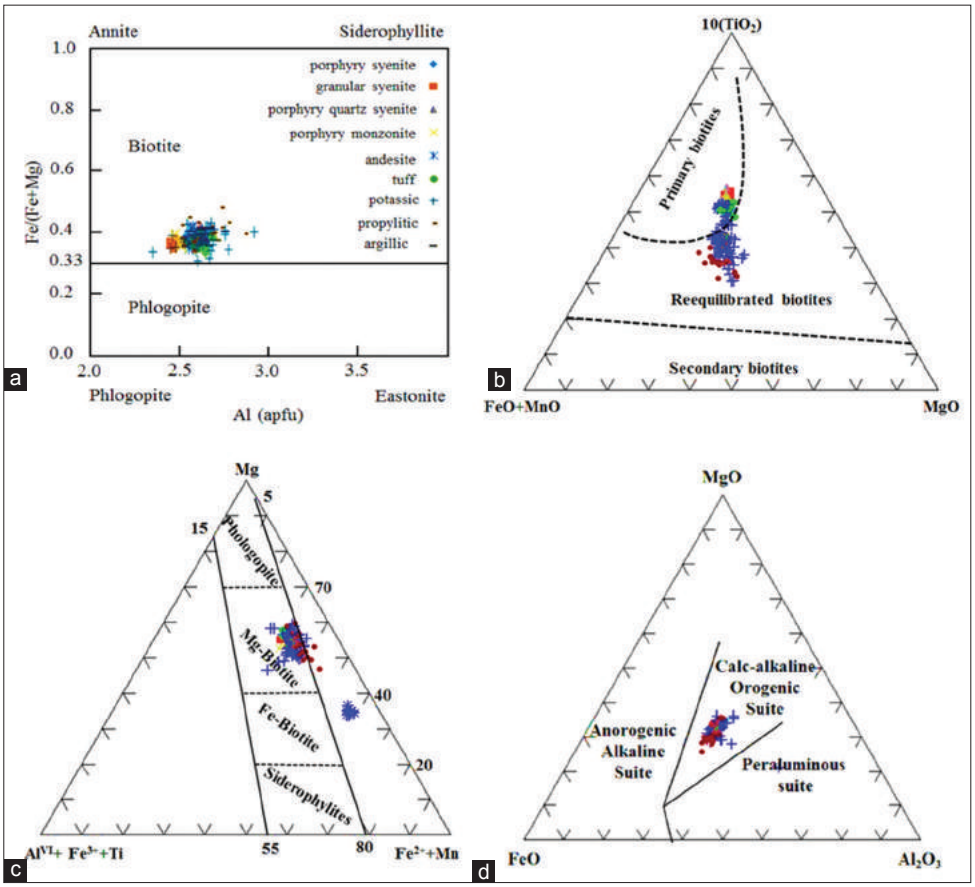

Figure 4: (a) Chemical composition of the Lar prospect biotites in the plots of (a) ΣAl versus Fe/(Fe+Mg) from Rieder *et al.,*[28] (b) 10*TiO_2–(FeO+MnO)–MgO from Nachit *et al.,*[30] (c) Mg–(Fe^{2+}+Mn)–(Al^{VI}+Fe^{3+}+Ti) from Foster,[36] (d) FeO-MgO-Al_2O_3 from Abdel-Rahman[37]

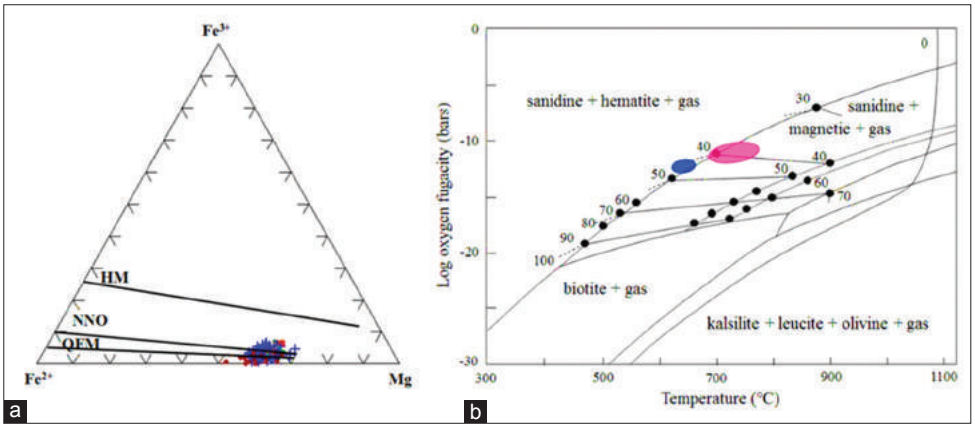

Figure 5: Plot of (a) variations of Fe^{3+}–Fe^{2+}–Mg in biotite collected from the Lar prospect igneous rocks; diagram after Wones and Eugster;[38] Fe^{3+} calculated according to Dymek,[10] (b) Log $f(O_2)$ – T for the biotite stability as a function of Fe/(Fe+Mg) ratio at total pressure of 2070 bars.[31] Curve labelled 0 represents maximum phlogopite stability and area bounded by curve labelled 100 is the annite stability field. The pink- and blue-colored areas are chemical composition of the Lar primary and secondary biotites. Similar symbols as in Figure 4

• $\log (f_{HF})/(f_{HCl})^{fluid}=-1000/T\ (1.22+1.65\ (X_{Mg})^{biotite}) +0.25+\log (X_F/X_{Cl})^{biotite}$.

Where X_F, X_{Cl}, and X_{OH} are the mole fractions of F, Cl, and OH in the hydroxyl site of biotite, respectively, $(X_{Mg})^{biotite}$ is the sum of Mg/sum octahedral cations, and T is the temperature in Kelvin for the halogen exchange. The log $(f_{H2O})/(f_{HF})$, log $(f_{H2O})/(f_{HCl})$, and log $(f_{HF})/(f_{HCl})$ ratios for fluids equilibrated with the Lar biotites were calculated using equations of Munoz (1992), estimated temperatures and fluorine and chlorine contents [Table 1], and were illustrated in Figure 6. According to Figures 6a and b, there are two distinct trends in log $(f_{H2O})/(f_{HF})$, log$(f_{H2O})/(f_{HCl})$, and log $(f_{HF})/(f_{HCl})$ ratios in the granular and porphyroid igneous rocks.

The porphyroid igneous rocks have different and higher ratios of log $(f_{H2O})/(f_{HF})$, log $(f_{H2O})/(f_{HCl})$, and log $(f_{HF})/(f_{HCl})$, indicating the fact that they were probably affected by later meteoric water reaction on exchangeable sites. In other words, orthomagmatic fluids first caused the potassic alteration in the Lar porphyroid igneous rocks; then, influx of meteoric water caused the dissolution of early-formed copper sulfides, resulting in remobilization of Cu-Mo into the silicic veins. This may suggest that the granular rocks were not/or less affected by the hydrothermal fluids which are responsible for Cu-Mo mineralization. Furthermore, the halogen-fugacity ratios in potassic, propylitic, and argillic alterations are distinctive from each other [Figure 6c and d]. According to different halogen-fugacity ratios of biotite indicate different temperature, pressure, and fluid composition.

In general, biotites that were formed under the same physicochemical conditions will produce linear chemical trends on the log (X_F/X_{OH}), log (X_{Cl}/X_{OH}), and log (X_{Cl}/X_F) versus X_{Mg} diagrams (Zhu and Sverjensky, 1992).[33] Based on Figure 7, the chemical compositions of log (X_F/X_{OH}), log (X_{Cl}/X_{OH}), and log (X_F/X_{Cl}) versus X_{Mg} from the Lar biotites

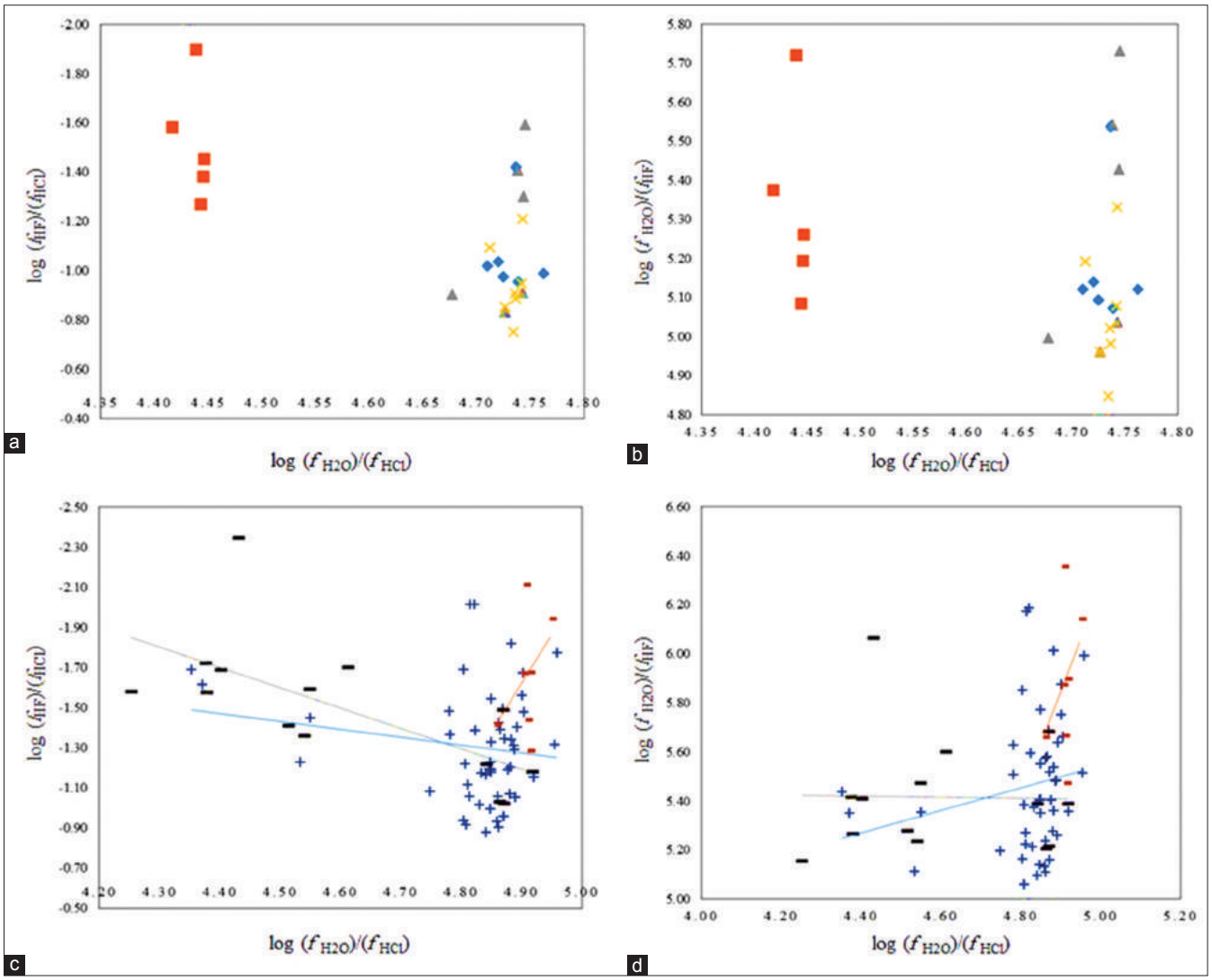

Figure 6: (a) Relationships of biotite halogen contents in and (b) porphyroid and granular igneous rocks, (c and d) alteration areas of the Lar Cu-Mo prospect. Similar symbols as in Figure 4

show different trends of composition. On the other hand, different slopes suggest that the chemical compositions of biotites were influenced by varying halogen-bearing fluids, variation in fO_2 and fS_2 of the fluids, and wall rock and hydrothermal fluids reactions.

X_{Mg}, X_{sid}, and X_{an} of the biotite from the Lar prospect were used to calculate the halogen intercept values such as IV (F), IV (Cl), and IV (F/Cl), respectively, using the following equations of Munoz:[39]

- $IV(F)^{biotite}=1.52\ X_{Mg}+0.42\ X_{an}+0.20\ X_{sid}-\log(X_F/X_{OH})$,
- $IV(Cl)^{biotite}=-5.01-1.93\ X_{Mg}-\log(X_{Cl}/X_{OH})$.

Where X_{Mg}, X_{sid}, and X_{an} in biotite were obtained from Gunow *et al*. (1980)[40] as follows:

- $X_{sid}=[(3-Si/Al)/1.75]\ (1-X_{Mg})$
- $X_{an}=1-(X_{Mg}+X_{sid})$.

The IV (Cl) of the granular igneous rocks is more negative than porphyroid type, and IV (F) and IV (F/Cl) values in porphyroid igneous rocks are less than the granular type [Table 1].

The Lar biotite intercept values of F, Cl, and F/Cl are consistent with other porphyry copper deposits of (IV (F) (1.1-3.0) and IV (F/Cl) (4.60-7.0).[41-43] Although the halogen fugacity and intercept values of the Lar biotites fall into the field of the Sarcheshmeh porphyry copper deposit, the IV (Cl) of later tends to be more Cl-rich than the Larsample [Figure 8]. Moreover, the Sarcheshmeh porphyry copper deposit was formed by the hydrothermal activity related to a sub-volcanic Miocene granodioritic stock, which introduces the Eocene andesitic volcanic and granitoids sequence;[44] however, the Lar Cu-Mo prospect is related to the shoshonitic intrusions that intruded to the volcanic rocks of the Oligocene LIC.

CONCLUSION

The Lar Cu-Mo prospect was formed by the hydrothermal activity related to the syenitic to monzonitic porphyroid igneous rocks with shoshonitic nature which introduces the LIC volcanic sequence. The hydrothermal alterations are limited and occurred as silicic, potassic, phyllic, propylitic, and argillic. Hypogene sulfide minerals mainly occur as disseminated and sulfidic and silicic veins and veinlets consisting of chalcopyrite, bornite, molybdenite, and minor pyrite. Biotite as main ferromagnesian mineral of host rocks occurs as primary in less altered rocks and secondary in the alteration areas.

The Lar biotites are Mg- and Ti-rich and F- and Cl-poor and mainly fall within the field close to the phlogopite–biotite

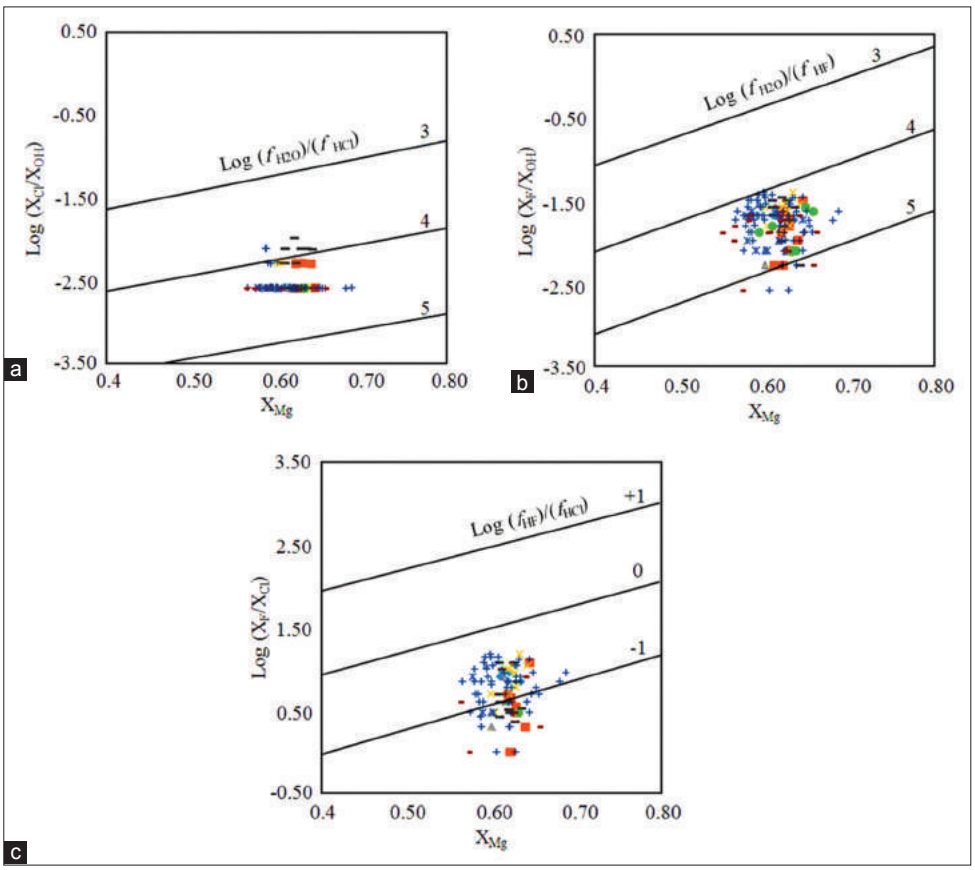

Figure 7: Plot of X_{Mg} versus (a) log (X_F/X_{OH}), (b) log (X_{Cl}/X_{OH}), and (c) log (X_F/X_{Cl}) for the Lar Cu-Mo prospect biotites. Similar symbols as in Figure 4

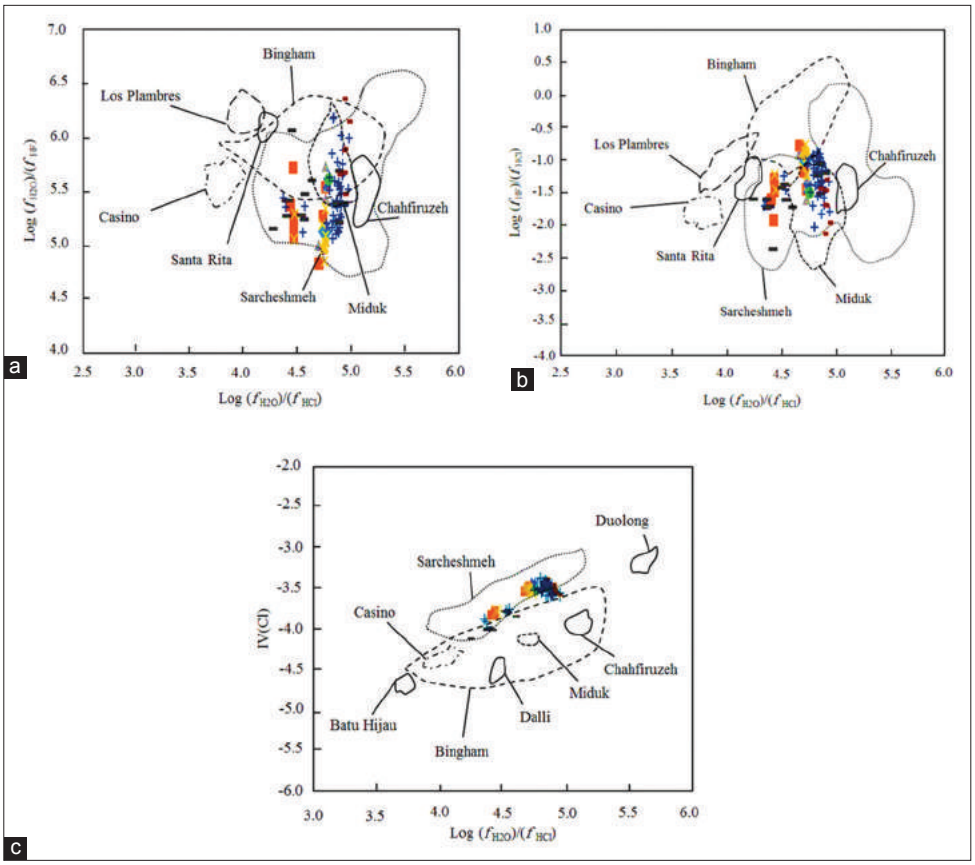

Figure 8: Comparison of the Lar prospect igneous rocks with the other intrusions associated with porphyry-style systems in terms of a) log (fH2O/fHCl) versus log (fH2O/fHF), b) log (fH2O/fHCl) versus log (fHF/fHCl), and c) log (fH2O/fHCl) versus IV (Cl) values. Data for other intrusions: Bingham (Lanier et al., 1978; Parry et al., 1978; Bowman et al., 1987)[45-47] Casino (Selby and Nesbitt, 2000)[11], Miduk (Boomeri et al., 2009), Sarcheshmeh (Boomeri et al., 2010)[48], Los Pelambres (Taylor, 1983)[41] and Santa Rita (Jacobs and Parry, 1979)[49]. Similar symbols as in Figure 4.

boundary composition. The high Mg and low Al^{VI} contents of the Lar biotites reflect a slightly fractionated magma. Calculated halogen fugacity and F, Cl, and F/Cl intercept values of the Lar biotites are consistent with porphyry-style mineralization system. The weak correlations, especially between halogen fugacity in the biotite structure of the porphyroid (ore-bearing) and granular (barren) igneous rocks, and primary and secondary biotites indicate that the biotite has been equilibrated with a heterogeneous fluid or mixing of magmatic and meteoric fluids occurred in the Lar prospect. The trend of the biotite chemistry across iso-fugacity ratio contours (parallel lines representing the calculated log (f_{H2O}/f_{HF}), log (f_{H2O}/f_{HCl}) and log (f_{HF}/f_{HCl})) also indicates that these biotites were equilibrated with different fluids. It seems that orthomagmatic fluids first caused the potassic alteration in the Lar porphyry intrusions. Then, influx of meteoric water caused the dissolution of early-formed copper sulfides, resulting in remobilization of Cu-Mo into the silicic veins.

REFERENCES

1. Chance P. Petrogenesis of a low-Ti, Potassic Suite: Kuh-e Lar Caldera Subsidence Complex, Eastern Iran. M.Sc.Thesis. Western Ontario Univ (London); 1981.
2. Bagheri S, Bakhshi MR. Investigation of North Zahedan Magmatism and its Relation to ore genesis, Published Research Report. Zahedan Iran: University of Sistan and Baluchestan; 2001.
3. Ghafari-Bijar S. Geochemistry of Potassic Mafic Rocks in the Lar Complex, North of Zahedan, East of Iran, M.Sc. Thesis, Sistan and Baluchestan Univ; 2009.
4. Soltanian A. Petro genesis of Volcanic Rocks from Lar Complex, North of Zahedan, East of Iran, M.Sc. Thesis, Sistan and Baluchestan Univ; 2013.
5. Karimi A. Geochemical behaviors and geological studies of copper and par agenesis elements in Lar mineralization (North Zahedan). Geos Sci Q J 2002;43:56-67.
6. Nakisa M. Summing up exploration of calculating Lar copper ore deposits, Zahedan. Ministry of Industries and Mines. Iran: National Iranian Copper Industries Company. 2002. p. 122.
7. Dushangani F. Mineralogy, Alteration and Origin of Cu Mineralization in Lar, North of Zahedan, East of Iran, M.Sc. Thesis, Sistan and Baluchestan Univ; 2015.
8. Moradi R. Geochemistry of the Lar Cu and Mo Deposit, North of Zahedan, Ph.D. Thesis, Sistan and Baluchestan Univ; 2016.

9. Imai A. Genesis of the mamut porphyry cu deposit, Sabah, east of Malaysia. Resour Geol 2000;50:1-23.
10. Selby D, Nesbitt BE. Chemical composition of biotitic from the Casino porphyry Cu-Au-Mo mineralization, Yukon, Canada: Evaluation of magmatic and hydrothermal fluid chemistry. Chem Geol 2000;171:77-93.
11. Xianwu B, Ruizhong H, Hanley JJ, Mungall JE, Jiantang P, Linbo S, *et al*. Crystallization conditions (T, P, fO_2) from mineral chemistry of Cu-and Au mineralized alkaline intrusions in the Red River-Jinshajing alkaline igneous belt, western Yunnan province, China. China Mineral Petrol 2009;96:43-58.
12. Siahcheshm K, Calagari AA, Abedini A, Lentz DR. Halogen signatures of biotitic from the Maher-Abad porphyry copper deposit, Iran: Characterization of volatiles in syn-to post-magmatic hydrothermal fluids. Int Geol Rev 2012;54:1353-68.
13. Stöcklin J. Structural history and tectonics of Iran. A review. Am Assoc Petrol Geol Bull 1968;52:1229-58.
14. Tirrul R, Bell LR, Griffis RJ, Camp VE. The Sistan suture zone of eastern Iran. Geol Soc Am Bull 1983;94:134-50.
15. Kan Iran Engineering. Report of the Lar Copper Deposit Geological Map. National Iranian Copper Industries Co (NICICO); 1999.
16. Camp VE, Griffis RJ. Character, genesis and tectonic setting of igneous rocks in the Sistan Suture Zone, eastern Iran. Lithos 1982;15:221-39.
17. Sahebzadeh B. Petrography and Petrology of Igneous Intrusive of Zahedan-Lochan, M.Sc. Thesis, Islamic Azad Univ; 1996.
18. Hosseini MR. Petrology and geochemistry of SW-Zahedan Granitoids, M.Sc.Thesis, Tehran Univ; 2002.
19. Kord M. Petrology and Geochemistry of Cheshme bid Granitoids, Southeast of Zahedan, M.Sc.Thesis, Shahrood University of Technology; 2005.
20. Sadeghian M. Magmatism, Metallogeny and Emplacement Mechanisms of Zahedan Granitoidic Pluton, Ph.D. Thesis, Tehran Univ; 2005.
21. Sadeghian M, Bouchez JL, Nedelec A, Siqueira R, Valizadeh MV. The granite pluton of Zahedan (Southeast of Iran): A petro logical and magnetic fabric study of a nontectonic sill emplaced in a trans tensional setting. J Asian Earth Sci 2005;25:301-27.
22. Sadeghian M, Valizadeh MV. Emplacement mechanism of Zahedan granitoidic pluton with the aid of AMS method. J Earth Sci 2007;17:126-43.
23. Rahnama-Rad J, Sahebzadeh B, Mirhajizadeh AA. Weathering and weakness of Zahedan granitoids: A rock engineering point of view. Appl Geol 2008;4:247-57.
24. Ghasemi H, Sadeghian M, Kord M, Khanalizadeh A. The evolution mechanisms of Zahedan granitoidic batholith, southeast Iran. Iranian J Crystallogr Mineral 2010;17:551-78.
25. Moradi R, Boomeri M, Bagheri S. Petrography and geochemistry of intrusive rocks in the Shurchah antimony-bearing area Southeast of Zahedan. J Petrol (Isfahan University) 2014;5:15-32.
26. Farhoudi G, Karig DE. Makran of Iran and Pakistan as an active arc system. J Geol 1977;5:664-8.
27. Rieder M, Cavazzini G, D'Yakonov YS, Frank-Kamenetskii VA, Gottardi G, Guoggenheim S, *et al*. Nomenclature of the micas. Can Mineral 1998;36:905-12.
28. Luhr JF, Carmichael IS, Verekamp JC. The 1982 eruptions of El Chichon Volcano, Chiapas, Mexico: Mineralogy and petrology of the anhydrite-bearing pumices. J Volcanol Geoth Res 1984;23:69-108.
29. Douce AE. Titanium substitution in biotitic: An empirical model with applications to thermometry, O_2 and H_2O barometers, and consequence for biotitic stability. Hem Geol 1993;108:132-62.
30. Wones DR, Eugster HP. Stability of biotitic: Experiment, theory and application. Am Mineral 1965;50:1228-72.
31. Ague JJ, Brimhall GH. Magmatic arc asymmetry and distribution of anomalous plutonic belts in the batholiths of California: Effects of assimilation, cantonal thickness and depth of crystallization. Geol Soc Am Bull 1988;100:912-27.
32. Zhu C, Sverjensky DA. Partitioning of F-Cl-OH between biotitic and apatite. Geochim Cosmochim Acta 1993;56:3435-67.
33. Munoz JL. Calculation of HF and HCl fugacities from biotitic compositions: Revised equations. Geol Soc Am 1992;24:A221.
34. Nachit H, Ibhi A, Abia EH, Ohoud MB. Discrimination between primary magmatic biotitic, re-equilibrated biotitic and informed biotitic. CR Geosci 2005;337:1415-20.
35. Foster MD. Interpretation of the composition of trioctahedral micas. U.S. Geological Survey Professional 1960;354B:1-49.
36. Abdel-Rahman AM. Nature of biotitic from alkaline, calcalkaline, and per aluminous magmas. J Petrol 1994;35:525-41.
37. Dymek R. Titanium, aluminum and interlayer action substitutions in biotitic from high-grade gneisses West Greenland. Am Mineral 1983;68:880-99.
38. Munoz JL. F–OH and Cl–OH exchange in mica with application to hydrothermal ore deposits. Rev Mineral Geochem 1984;13:469-93.
39. Gunow AJ, Ludington S, Munoz JL. Fluorine in micas from the Henderson molybdenite deposits, Colorado. Econ Geol 1980;75:1127-37.
40. Taylor RP. Comparison of biotitic geochemistry of Bakircay, Turkey, and Los Pelambres, Chile, porphyry copper systems. J Min Metall 1983;92:B16-22.
41. Loferski PJ, Ayuso RA. Petrography and mineral chemistry of the composite Deboullie pluton, northern Maine, U.S.A.: Implications for the genesis of Cu–Mo mineralization. Chem Geol 1995;123:89-105.
42. Yavuz F. Evaluating micas in petrologic and metallogenic aspect: Part II-applications using the computer program $Mica^+$. Comput Geosci 2003;29:1215-28.
43. Boomeri M, Nakashima K, Lentz DR. The sarcheshmeh

porphyry copper deposit, Kerman, Iran: A mineralogical analysis of the igneous rocks and alteration zones including halogen element systematic related to cu mineralization processes. Ore Geol Rev 2010;38:367-81.
44. Lanier G, Raab WJ, Folsom RB, Cone S. Alteration of equigranular monzonite, Bingham Mining district, Utah. Econ Geol 1978;73:1270-86.
45. Parry WT, Ballantyne GH, Wilson JC. Chemistry of biotitic and apatite from a vesicular quartz latte porphyry plug at Bingham, Utah. Econ Geol 1978;73:1308-14.
46. Bowman JR, Parry WT, Kropp WP, Kruer SA. Chemical and isotopic evolution of hydrothermal solutions at Bingham, Utah. Econ Geol 1987;82:395-428.
47. Boomeri M, Nakashima K, Lentz DR. The miduk porphyry Cu deposit, Kerman, Iran: A geochemical analysis of the potassic zone including halogen element systematics related to cu mineralization processes. J Geochem Explor 2009;103:17-29.
48. Jacobs DC, Parry WT. Geochemistry of biotitic in the Santa Rita porphyry copper deposit, New Mexico. Econ Geol 1979;74:860-87.
49. Farokh-Nezhad M. Geochemical Characterization of Potassic Mafic Rocks, Mennonites and Syenites from Lar Complex, Eastern Iran, M.Sc. Thesis, Sistan and Baluchestan Univ; 2011.

Source of Support: Nil. **Conflict of Interest:** None declared.